Available online at www.sciencedirect.com
ScienceDirect
Trans. Nonferrous Met. Soc. China 35(2025) 552−562
Transactions of Nonferrous Metals Society of China
www.tnmsc.cn

Enhancement of piezoelectric properties with high Curie temperature in $CaBi_2Nb_2O_9$ via MnO_2 doping

Meng-si WANG[1], Yan ZHANG[1], Xiao-gang LUO[1], Lin TANG[1], Shan XIANG[1], Ru GUO[2], Xue-fan ZHOU[1], Ke-chao ZHOU[1], Dou ZHANG[1]

1. State Key Laboratory of Powder Metallurgy, Central South University, Changsha 410083, China;
2. Department of Mechanical and Automation Engineering, The Chinese University of Hong Kong, Hong Kong 999077, China

Received 30 June 2024; accepted 24 December 2024

Abstract: MnO_2-doped $Ca_{0.97}Bi_{2.03}Nb_2O_9$ ceramics with greatly improved piezoelectric performance were prepared via conventional solid state sintering method. The effects of MnO_2 doping on the microstructure and electrical properties of $Ca_{0.97}Bi_{2.03}Nb_2O_9$ ceramics were studied. X-ray diffraction (XRD) analysis and Rietveld refinement revealed a reduction in orthorhombicity with MnO_2 doping, which contributed to the enhancement of the piezoelectric properties. Furthermore, the introduction of MnO_2 lowered the sintering temperature, thereby reducing the formation of oxygen vacancies in the ceramic. The optimal performance was achieved in the $Ca_{0.97}Bi_{2.03}Nb_2O_9$−0.3wt.%$MnO_2$ sample, exhibiting a piezoelectric coefficient (d_{33}) of 13.6 pC/N, a DC resistivity of 3×10^6 Ω·cm at 500 °C, and a Curie temperature of 965 °C. Additionally, all doped samples demonstrated excellent thermal stability over a wide temperature range, from room temperature to 900 °C.

Key words: $CaBi_2Nb_2O_9$ ceramics; MnO_2 doping; crystal structure; oxygen vacancy

1 Introduction

There is an increasing demand for high temperature piezoelectric devices in various areas, including aerospace, aircraft, automotive and power-generating [1−5]. Piezoelectric materials for high-temperature applications are required to own a high Curie temperature (T_C) to withstand the high working temperature and good piezoelectric coefficient (d_{33}) to ensure sensitivity [6,7]. However, the temperature limit of conventional lead zirconate titanate (PZT) is around 380 °C, and the lead volatilization during the ceramic preparation process is harmful to the environment [8,9]. Therefore, research on lead-free piezoelectric materials for high temperature applications is of great importance [10].

Bismuth layer-structured ferroelectrics (BLSFs), also known as Aurivillius-phase materials, are considered as promising candidates for future high-temperature applications due to their high T_C, good thermal depolarization performance and high resistivity [11−13]. The general formula of BLSFs presents as $(Bi_2O_2)^{2+}(A_{m-1}B_mO_{3m+1})^{2-}$, where m represents the number of octahedral layers between adjacent $(Bi_2O_2)^{2+}$ layers [14]. $CaBi_2Nb_2O_9$ (CBN) exhibits a rather high T_C of 940 °C among the BLSFs family, which is an ideal material for high temperature usage [13]. However, it is difficult for

Corresponding author: Yan ZHANG, Tel: +86-13787257957, E-mail: yanzhangcsu@csu.edu.cn;
Ru GUO, Tel: +86-15200866154, E-mail: ruguo@cuhk.edu.hk
DOI: https://doi.org/10.1016/S1003-6326(24)66699-9

CBN to be polarized due to the restriction of spontaneous polarization in $a-b$ plane, resulting in a high coercive field and thus a low piezoelectric performance [15,16]. The low d_{33} of ~5 pC/N largely hinders the practical application of CBN ceramics [17].

To enhance the piezoelectric properties of $CaBi_2Nb_2O_9$ (CBN), researchers have focused extensively on chemical and structural modifications, including ion doping and grain orientation. Textured CBN ceramic through spark plasma sintering (SPS) method has been reported by YAN et al [13] to obtain a d_{33} value up to 19.5 pC/N. Although a relatively high d_{33} can be realized, grain orientation technique is difficult to be applied in market due to the large cost of processing. Hence, chemical doping is a better choice for piezoelectricity enhancement of CBN. Many researches have been done in recent years, including *A*-site, *B*-site cation substitution, and AB-site co-doping, which can enhance the d_{33} to 12−18 pC/N [18−23]. It has been revealed that the A-site doping would result in a distinct structural distortion, such as pseudo-tetragonal distortion and $[NbO_6]$ octahedron tilting, and thus lead to an improvement in piezoelectric constant while the *B*-site doping usually plays a role to enhance the thermal stability of BLSFs [9,24,25]. However, most studies on ion doping have reported an improvement in d_{33}, accompanied by a simultaneous reduction in T_C. Achieving high piezoelectric performance while maintaining a high T_C is crucial for the practical application of CBN-based ceramics.

The Bi element tends to volatilize during the sintering process of CBN, resulting in the formation of numerous oxygen vacancies and degrading the insulation resistance [26]. Therefore, reducing the bismuth volatilization is an effective method to promote the electrical properties of CBN [27]. Moreover, researchers have reported that sintering additives can hinder the volatilization of Bi element by lowering the sintering temperature [28,29]. As a multiple-valence oxide, MnO_2 has been used to promote the electrical properties of piezoelectric materials [30−35]. In previous work, a simple Bi^{3+} self-doping showed the ability to construct pseudo-tetragonal phase boundary to enhance electrical properties of CBN ceramics [27].

In this study, different amounts of MnO_2 were added to $Ca_{0.97}Bi_{2.03}Nb_2O_9$ ceramics. Excess Bi can compensate for the loss of Bi during the sintering process and help modulate structural distortion. Additionally, the MnO_2 additive lowers the sintering temperature, further preventing Bi volatilization at high temperatures. The addition of MnO_2 also induces distortion in the lattice structure of CBN-based ceramic. The effects of MnO_2 on the phase structure, lattice distortion, defect concentration, and electrical properties are systematically investigated in this work. And it provides a new approach to fabricate CBN-based ceramics with ultra-high Curie temperature and good piezoelectric properties.

2 Experimental

Ceramic samples $Ca_{0.97}Bi_{2.03}Nb_2O_9$–$x$wt.%$MnO_2$ (x=0, 0.1, 0.2, 0.25, 0.3 and 0.4, abbreviated as CBN–xMn) were prepared by a conventional solid-state sintering method. At first, raw materials including $CaCO_3$ (99.9%, Aladdin), Bi_2O_3 (99.9%, Macklin) and Nb_2O_5 (99.9%, Aladdin) were weighed according to the stoichiometric ratio of CBN and then ball milled with alcohol for 24 h. The mixed powder was pre-sintered at 850 °C for 2 h after drying at 80 °C overnight. MnO_2 (99.95%, Aladdin) was added to the CBN powders with the proportion of 0, 0.1, 0.2, 0.25, 0.3 and 0.4 wt.% followed by ball milling with alcohol for 24 h and drying overnight. Subsequently, the mixture was granulated using 5 wt.% polyvinyl alcohol (PVA) and pressed into discs with a diameter of 10 mm and thickness of about 1 mm. Finally, the discs were sintered at 1100 °C (doped samples) and 1150 °C (undoped ones) for 4 h after burning off the binders at 550 °C. Here, the sintering temperature of undoped samples is higher because MnO_2 can act as a sintering aid to lower the sintering temperature and improve sintering performance. For comparison, the undoped ceramic samples sintered at 1100 °C were also prepared and characterized, and the results are shown in Fig. S1 in Supporting Information.

The phase structure of the ceramic samples was tested by X-ray diffractometer (XRD, Smart lab, Japan) using Cu K_α radiation (λ=0.15406 nm) from 5 to 120 °C with a rate of 5 °C/min. The

microstructure of the samples was observed by the field-emission scanning electron microscopy (SEM, Nova Nano SEM230, FEI Electron Optics B.V, Czech Republic) after polishing and hot corrosion. X-ray photoelectron spectroscopy (XPS, Kratos AXIS SUPRA+, Japan) was applied to determining the chemical composition and valance states of the samples. The ferroelectric domain structure was observed via atomic force microscope (Nanoman TM VS, USA) in the piezoelectric response mode at room temperature. Ferroelectric properties including polarization−electric field (P–E) and current−electric field (I–E) hysteresis loops were obtained by the ferroelectric analyzer (aixACCT Analyzer TF3000) at a temperature of 150 °C. The DC resistivity data varying from room temperature to 800 °C was measured by a test system (RMS−1000P, Partulab, China). The temperature dependence of the permittivity and dielectric loss was measured by a TZDM system connected to program-controlled furnace. The frequency-dependent room-temperature permittivity of poled samples was tested by the LCR meter (Agilent 4294A). Samples were poled in silicon oil at 180 °C for 1 h applying the electric field of 180 kV/cm and then the piezoelectric coefficient (d_{33}) of these poled samples was measured by the quasi-static piezometer (ZJ-6, Institute of Acoustics, Chinese Academic of Science, Beijing, China) at room temperature. The poled samples were annealed at a series of temperatures for 2 h to evaluate the thermal stability of the ceramic samples.

3 Results and discussion

3.1 Phase and microstructure

To investigate the structural variations of CBN-based ceramics with different MnO_2 doping contents, the XRD data for the powder samples are shown in Fig. 1(a). The strongest reflection peak is shown at the (115) plane, which is in accordance with the fact that the most intense reflection plane of BLSFs is in (112m+1) [36,37]. No impurity phase was observed in the XRD data for all the samples, indicating that MnO_2 additives have successfully been incorporated into the crystal lattice of CBN-based ceramic. The magnified (020)/(200) peaks are given in Fig. 1(a), it shows that the (020)/(200) reflection peaks have a trend to merge into one peak with a higher doping content of MnO_2. It suggests a possible phase transition from orthorhombic to pseudo-tetragonal symmetry [38], which is further confirmed by the refined XRD data presented below.

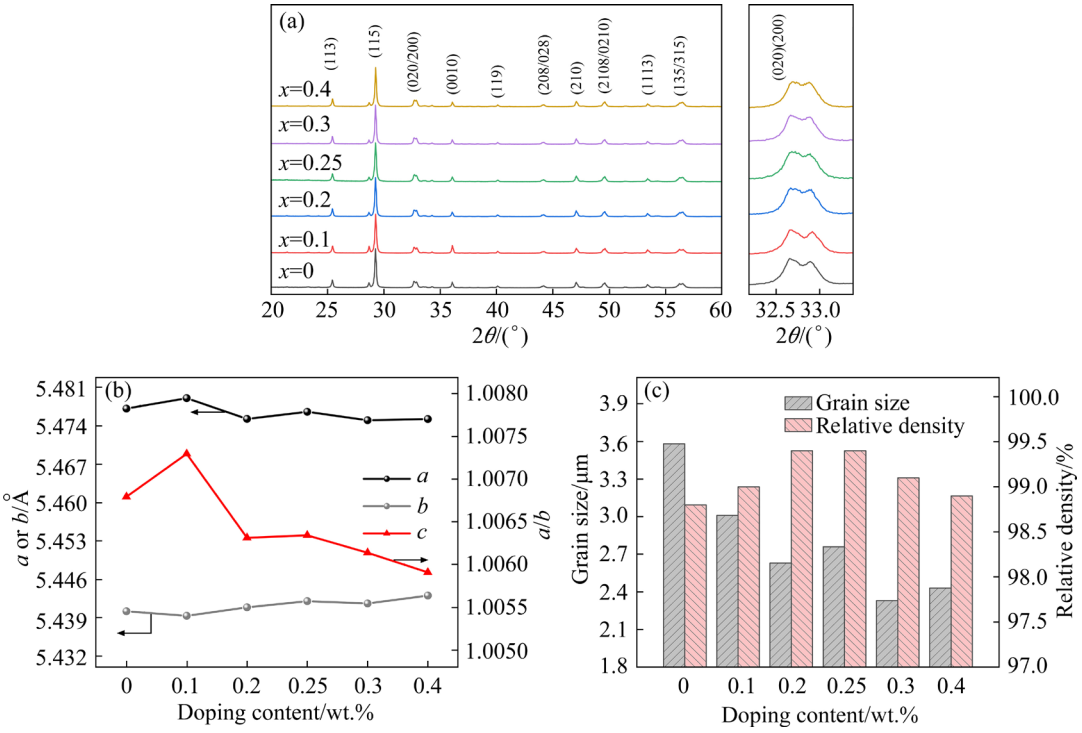

Fig. 1 XRD patterns and magnified (020)/(200) peaks of CBN-xMn ceramics (a), variations of cell parameters with MnO_2 doping content (b), and average grain size and relative density (c)

To further identify the lattice structure distortion of the CBN-*x*Mn samples, Rietveld refinement of powder XRD data was performed for all samples via Fullprof software using the $A2_1am$ space group. The calculated values are in good agreement with the experimental data supported by the reasonable reliability factors including R_{wp}, R_p and χ^2 as shown in the Fig. S2 in Supporting Information. And Fig. 1(b) displays the lattice parameters as a function of the doping levels. It can be observed that the lattice constant a increases when x increases from 0 to 0.1, and then declines as x further increases, while b decreases first and then gradually increases. The degree of structural distortion can be evaluated by the variation in the a/b ratio, as shown in Fig. 1(b). The value of a/b initially increases at a low doping level of x=0.1, then decreases with further increase in MnO_2 content. This suggests that an optimal level of MnO_2 doping is required to induce pseudo-tetragonal lattice distortion in the CBN-based ceramics [39].

The SEM images of the ceramics are displayed in Fig. 2. It can be observed that the CBN-*x*Mn ceramics possess plate-like grains and show strong anisotropy, which is due to the faster growth speed along $a-b$ plane than other directions [40]. Based on the SEM images in Fig. 2, the average grain size was calculated using Nano Measurer. As shown in Fig. 1(c), the variations in average grain size and relative densities indicate that MnO_2 doping leads to a reduction in grain size. It may be attributed to the suppression of oxygen vacancies in the ceramics due to the promotion of sintering process by MnO_2 additives [19]. It is known that the volatilization of Bi during the sintering process would generate the oxygen vacancies, which facilitates the diffusion process in the grains/grain boundaries and thus promoting the grain growth [41]. In this case, the addition of MnO_2 lowered the sintering temperature of CBN-based ceramics and inhibited the generation of oxygen vacancies, leading to the decreased grain size in the doped samples. Meanwhile, all samples exhibit high densities over 98% of the theoretical value owing to the dense microstructures of the samples shown in the SEM images. The domain structures of CBN-*x*Mn ceramics were measured by PFM, as shown in Fig. S3 in Supporting Information, nano-size domains are formed in these samples and small-sized domain is conducive to facilitate the response to external electric field [21,42]. It was noted that the domain size shows no significant change with the MnO_2 doping content.

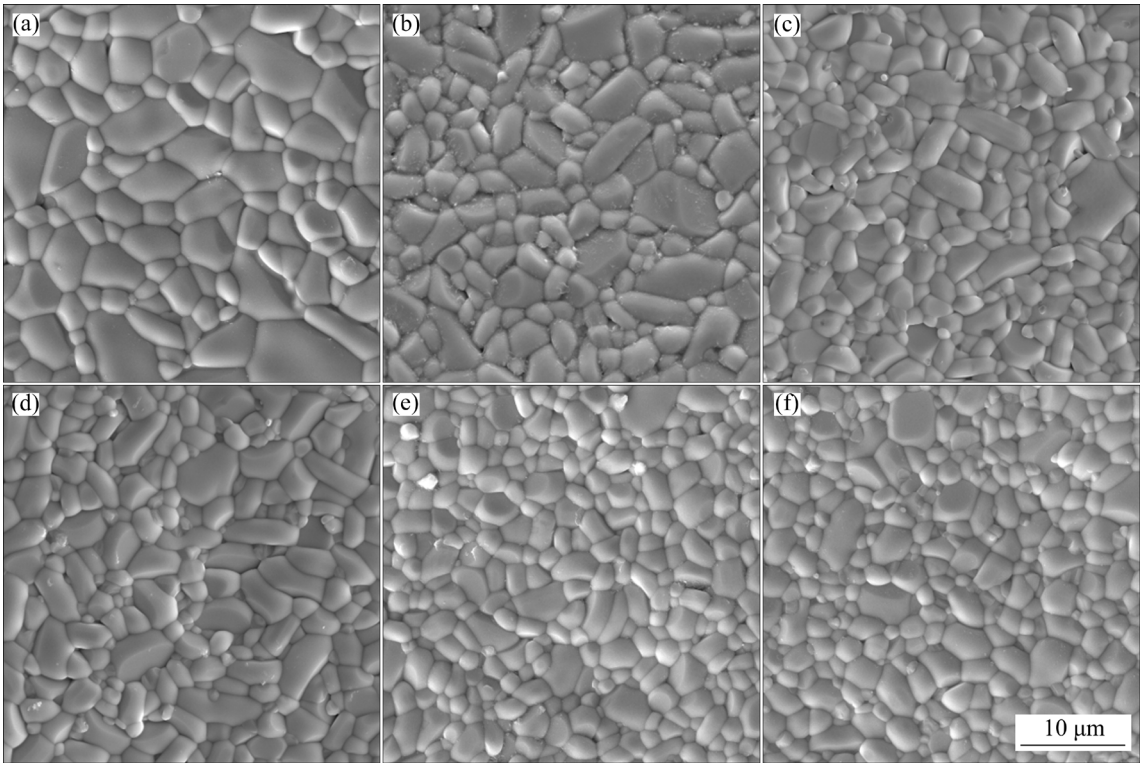

Fig. 2 Surface SEM images of CBN-*x*Mn ceramics: (a) x=0; (b) x=0.1; (c) x=0.2; (d) x=0.25; (e) x=0.3; (f) x=0.4

3.2 Defect

XPS measurements were performed to investigate the variation in oxygen vacancies in CBN-*x*Mn ceramics. As shown in Fig. 3, two independent peaks were obtained by peak fitting operation of the O 1s spectra. It can be observed that the experimental data are well-fitted using two binding energy peaks, where the peak at 529.7 eV represents lattice oxygen (O_L) in ceramics, and the peak located at 531.4 eV is the oxygen-deficient region (oxygen vacancy, V_O) [43]. The ratio of the peak areas between V_O and O_L can be used to quantify the oxygen vacancy concentrations in the ceramics [44]. In Fig. 3, peak area ratio of V_O/O_L declines from 0.311 to 0.276 with increasing content of MnO_2, which is in accordance with the declined grain size mentioned in Fig. 1(c). It reveals that MnO_2 plays a role to prohibit the volatilization of Bi and decrease the formation of oxygen vacancies [35].

3.3 Ferroelectric properties

Piezoelectric performance of ceramics is closely related to their ferroelectric behavior. To explore the piezoelectric properties, Figs. 4(a) and (b) show the *P*–*E* hysteresis loops and *I*–*E* curves at 150 °C of the CBN-*x*Mn ceramics under the same external electric field (190 kV/cm). It can be seen that all samples exhibit a typical open hysteresis loops and obvious switching current peaks. The remnant polarization (P_r), switching current peak (I_{max}) and coercive field ($E_{I_{max}}$) values of the samples with different MnO_2 doping contents are displayed in Figs. 4(c) and (d), respectively. The P_r decreases firstly when $x<0.2$ compared with the pristine one, then it keeps rising to achieve the maximum of 9.73 μC/cm^2 at $x=0.3$ and declines with excessive MnO_2 of 0.4 wt.%. Generally, the phase structure distortion plays an important role in the variation trend of P_r. The value of a/b shown in Fig. 1(b) increases when $x=0.1$, indicating an enhanced orthorhombicity and thus the decreased I_{max} and P_r. Furthermore, the increase of P_r and I_{max} can be seen when x increases from 0.1 to 0.3, which should be attributed to the easier polarization switching process due to the reduced orthorhombicity and enhanced pseudo-tetragonality. In Fig. 4(d), the variation of the $E_{I_{max}}$ with different MnO_2 doping contents shows a reverse trend with P_r and I_{max}. $E_{I_{max}}$ can reflect the resistance to domain switching [45], thus a low E_{Imax} is conducive to domain switching, contributing to high P_r and I_{max}.

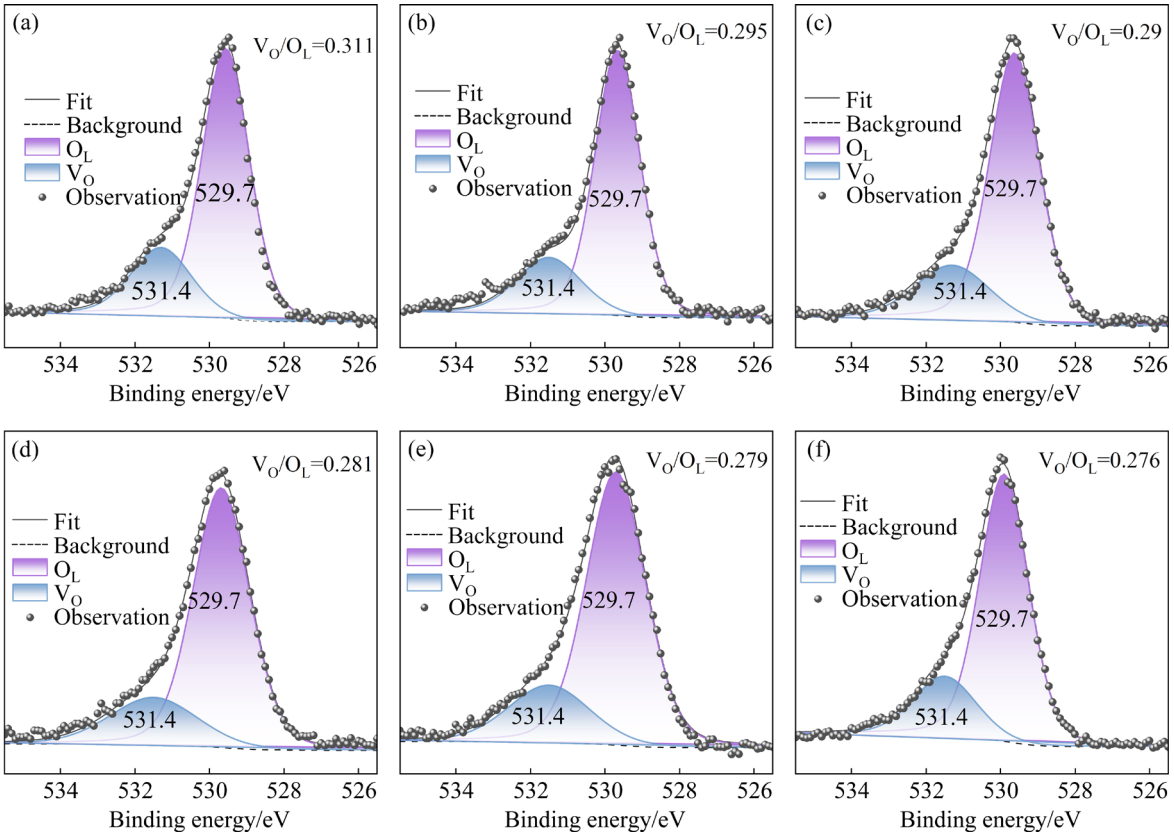

Fig. 3 XPS O 1s spectra of CBN-*x*Mn ceramics: (a) $x=0$; (b) $x=0.1$; (c) $x=0.2$; (d) $x=0.25$; (e) $x=0.3$; (f) $x=0.4$

3.4 Dielectric and piezoelectric properties

It has been revealed that the factors related to the piezoelectric coefficient (d_{33}) can be expressed as $d_{33}=Q\varepsilon_0\varepsilon_r P_r$ [46], the frequency-dependent dielectric constant (ε_r) after poling and the ε_r varying with different MnO_2 contents are shown in Fig. 5(a). The dielectric constant decreases firstly at x=0.1 and then increases when x rises, achieving the peak at x=0.3 (98.1). In general, higher P_r and ε_r values are beneficial to the enhancement of piezoelectric coefficient. Figure 5(b) depicts the d_{33} of the CBN-xMn ceramics. Clearly, a rational doping of MnO_2 can promote the piezoelectricity of CBN-based ceramics, with the maximum d_{33} of 13.6 pC/N at x=0.3, which is consistent with the results of P_r and ε_r above.

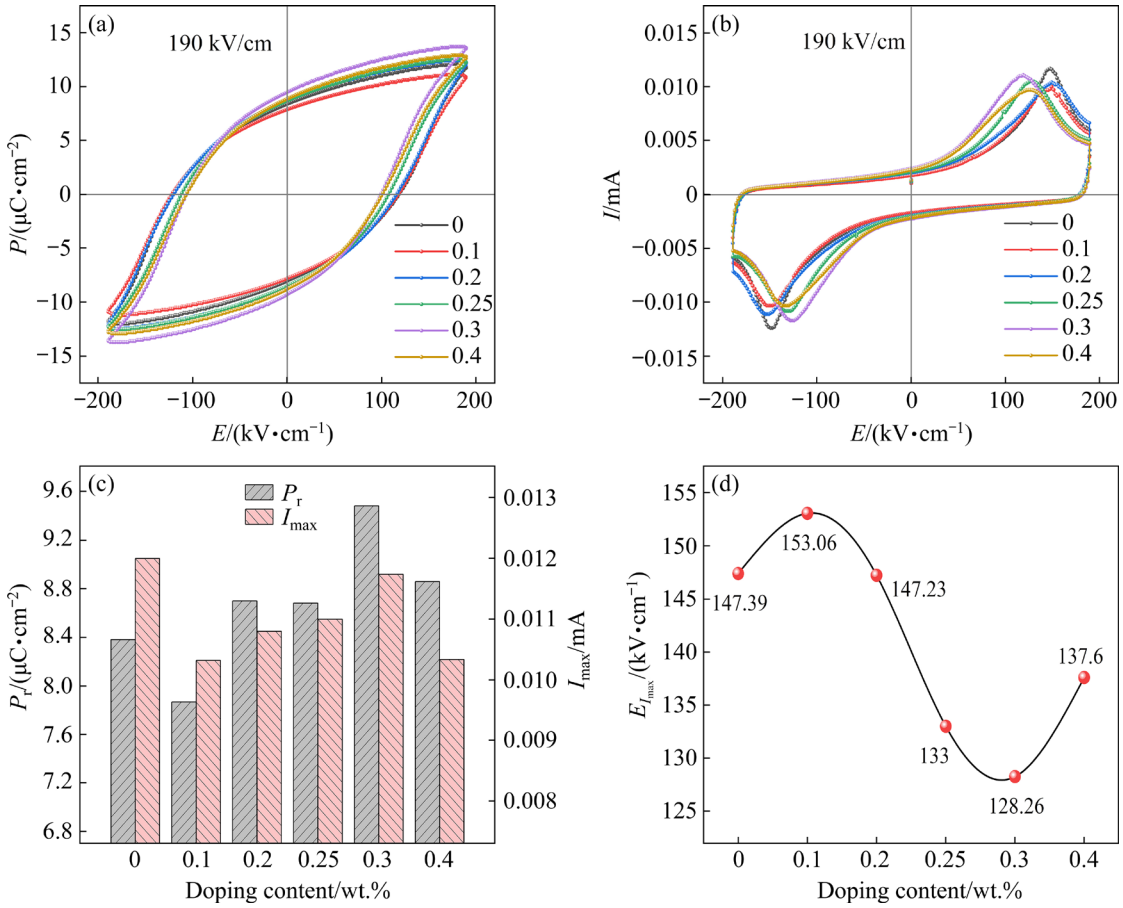

Fig. 4 P–E loops (a) and I–E loops (b) of CBN-xMn ceramics, and variation of P_r and I_{max} (c) and $E_{I_{max}}$ (d) with different MnO_2 doping contents

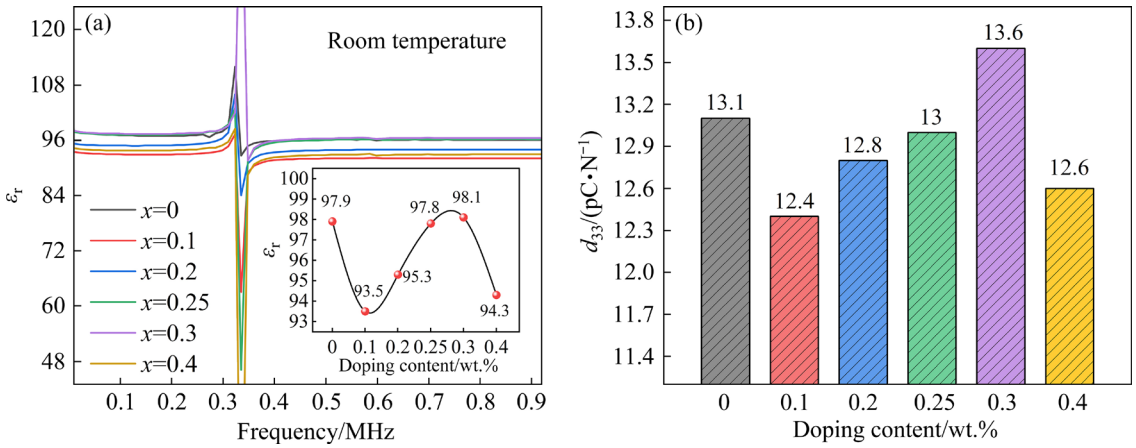

Fig. 5 Frequency-dependent ε_r of CBN-xMn ceramics after poling (a) and d_{33} values of CBN-xMn ceramics (b)

3.5 High-temperature performance

Figures 6(a, c) show the temperature-dependent dielectric constant and loss tangent of the CBN-*x*Mn ceramics measured at 1 MHz. With the temperature increasing, a clear dielectric peak can be seen in all samples, and the temperature corresponding to the peak is the Curie temperature (T_C), which is correlated to the phase transition from ferroelectric phase to paraelectric phase [47]. The variation trend of T_C with different doping contents is exhibited in Fig. 6(b). It can be observed that all samples display a relatively high T_C of over 958 °C and the T_C value shows an increasing trend after the doping of MnO_2, with the maximum value of 966 °C when x=0.4. Meanwhile, as shown in Fig. 6(b), all doped CBN-based ceramics show lower loss tangents of 0.05 at 500 °C compared with the pristine one, which is correlated to the suppressed oxygen vacancy concentrations by the addition of MnO_2 additives. In conclusion, the enhanced T_C along with the decreased loss tan δ indicates that the CBN-based ceramics modified by MnO_2 exhibit great potential in high temperature applications. In order to further detect the high temperature stability of the CBN-*x*Mn ceramics, thermal depolarization test was applied from room temperature to 980 °C to obtain the variation of piezoelectric coefficient during the annealing process. In Fig. 6(d), a slight change of d_{33} can be observed in these samples, which may be resulted by the unstable defect dipoles and reversible non-180° domains [48,49]. In general, all samples maintain a relatively stable d_{33} under 900 °C, and then drop sharply at around 960 °C, which is related to their Curie temperatures. The excellent thermal stability is conducive to the high temperature applications of CBN-*x*Mn ceramics.

High temperature resistivity is vital in terms of the piezoelectric performance of BLSFs, and it is generally known that the resistivity would decrease with increasing temperature due to the enhancement in mobility of both defect ions and intrinsic carriers at higher temperatures [50]. The temperature-dependent DC resistivity ρ_{dc} of CBN-*x*Mn ceramics is given in Fig. 7(a). The ρ_{dc} of MnO_2 doped CBN-based ceramics is higher than the undoped one at 300 °C when x<0.4, and a slight decline can be observed as the temperature rising after doping.

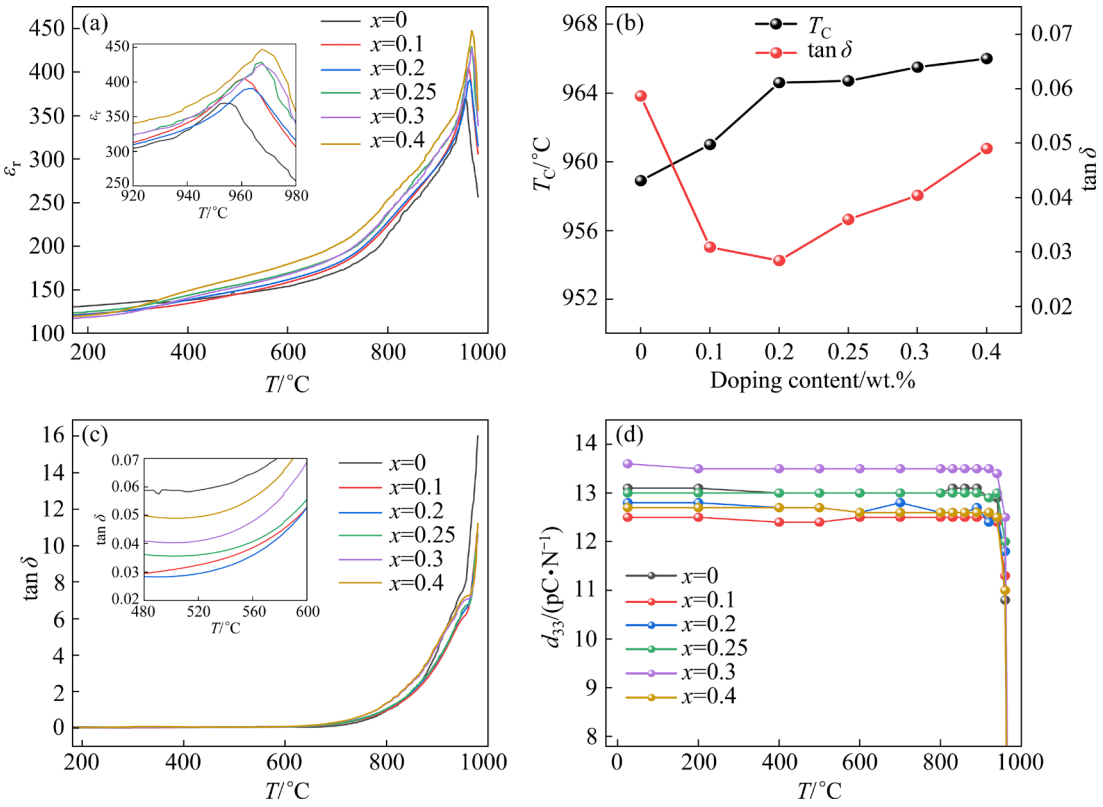

Fig. 6 (a, c) Temperature-dependent dielectric permittivity ε_r and dielectric loss tan δ of CBN-*x*Mn ceramics, respectively; (b) Curie temperature T_C and tan δ at 500 °C; (d) Temperature dependence of d_{33} values of CBN-*x*Mn ceramics

It should be noted that the high content of doping when x=0.4 is harmful to the electrical resistivity because excessive MnO_2 may concentrate at the grain boundaries to cause defects. In conclusion, all the samples maintain a high resistivity over $1\times10^6\ \Omega\cdot$cm at 500 °C.

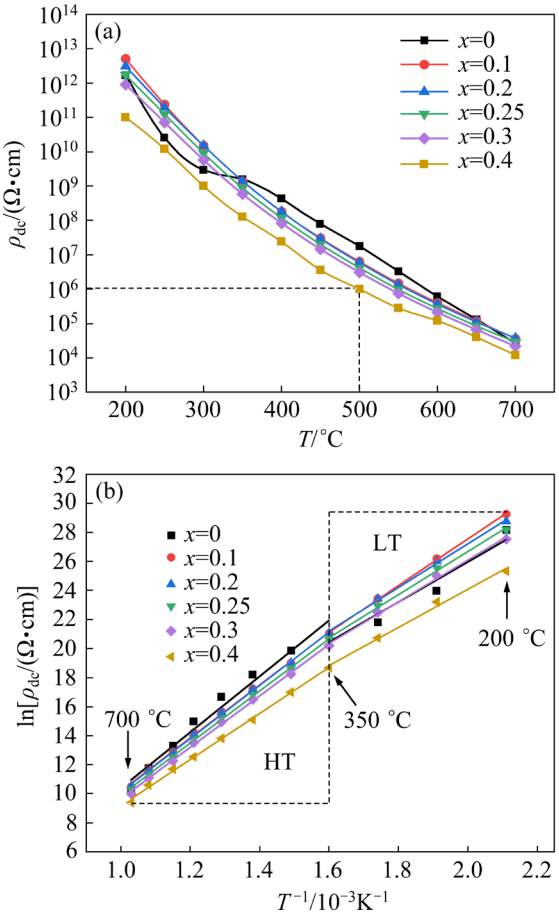

Fig. 7 (a) Temperature-dependent DC resistivity of CBN-xMn ceramics; (b) Fitted relationship between DC resistivity and temperature by Arrhenius function

To further study the mechanism of the variation of electrical resistivity, Arrhenius Law formula $\rho=\rho_0\exp[-E_a/(k_BT)]$ was applied to measuring the activation energy of the samples, where ρ_0 is the pre-exponential factor, E_a is the conductive activation energy, k_B is Boltzmann constant, and T is the absolute temperature [51]. The fitted plot of the DC resistivity as a function of the temperature is shown in Fig. 7(b), and the calculated activation energy results are listed in Table 1. It has been revealed that a high E_a value means a high electrical resistivity [52]. Bismuth layer-structured ceramics exhibit two different conductive mechanism, which are the extrinsic conduction and the intrinsic conduction respectively [53]. It can be observed that the fitting plots are divided into two temperature regions at 350 °C in Fig. 7(b). Theoretically, the extrinsic conduction in low temperature region (LT) ≤350 °C is dominated by the movement of defects ions (oxygen vacancies) and the intrinsic conduction in high temperature (HT) region ≥350 °C is dominated by electron-hole carriers in the ceramics [54]. The activation energy values are in the range of 1.13−1.38 eV at LT and 1.36−1.66 eV at HT. In LT region, the conductive behavior primarily comes from the evaporation of bismuth during sintering process as shown in the following equations [55]:

$$2Bi_{Bi}^{X}+3O_{O}^{X}\rightarrow 2V_{o}^{\cdot\cdot}+Bi_2O_3\uparrow \quad (1)$$

$$\frac{1}{2}O_2+V_{O}^{\cdot\cdot}\rightarrow O_{O}^{X}+2h^{\cdot} \quad (2)$$

Increased E_a values can be seen at LT, which is in agreement with the results of declined oxygen vacancies after MnO_2 doping. However, the E_a value of the pristine CBN-based sample is higher than that of the doped samples at HT, which may be ascribed to the defect dipoles induced by the doping of MnO_2. Generally, rational doping of MnO_2 is conducive to the enhancement of DC resistivity of the CBN based ceramic.

Table 1 Activation energy (E_a) of CBN- xMn ceramics at HT and LT

x	E_a (HT)/eV	E_a (LT)/eV
0	1.66	1.19
0.1	1.57	1.38
0.2	1.58	1.29
0.25	1.55	1.28
0.3	1.53	1.24
0.4	1.49	1.21

4 Conclusions

(1) Decreased orthorhombicity after MnO_2 doping was demonstrated through the XRD observation and Rietveld refinement. Compact grain structure was obtained in the CBN-xMn ceramics and grain refinement was achieved with the addition of MnO_2.

(2) The Bi content was modulated to compensate the volatilization loss of Bi and the sintering temperature was lowered through the

doping of MnO_2, contributing to decreased oxygen vacancies and greatly enhanced DC resistivity to $3\times10^6\ \Omega\cdot$cm at 500 °C.

(3) Largely enhanced piezoelectric coefficient of 13.6 pC/N was achieved, which is twice higher than that of the pure CBN. The doping of MnO_2 leads to decreased orthorhombic lattice distortion and enhanced pseudo-tetragonality, which is the origin of a high P_r value and thus contributing to the enhancement of d_{33} value.

(4) The increase of Curie temperature was discovered with the addition of MnO_2 content, achieving the maximum value of 966.5 °C when the addition content is 0.4 wt.%, which is about 25 °C higher than the pure CBN. Meanwhile, good thermal stability of piezoelectric response in the temperature range of room temperature to 900 °C was achieved in all MnO_2-doped samples.

CRediT authorship contribution statement

Meng-si WANG: Conceptualization, Validation, Formal analysis, Data curation, Investigation, Resources, Writing − Original draft, Writing − Review & editing; **Yan ZHANG** and **Ru GUO:** Supervision, Validation, Formal analysis, Writing − Review & editing, Funding acquisition, Resources; **Xiao-gang LUO**, **Lin TANG** and **Shan XIANG:** Supervision, Resources, Investigation, Conceptualization; **Xue-fan ZHOU:** Conceptualization, Supervision, Validation, Writing − Review & editing; **Ke-chao ZHOU** and **Dou ZHANG:** Funding acquisition, Resources.

Declaration of competing interest

The authors declare that they have no known competing financial interests or personal relationships that could have appeared to influence the work reported in this paper.

Acknowledgments

This work was supported by the National Key Research and Development Program of China (No. 2022YFB3807404), the State Key Laboratory of Powder Metallurgy, the National Natural Science Foundation of China (No. 52102150, 52302158), and Xiaomi Young Talents Program, China.

Supporting Information

Supporting Information in this paper can be found at: http://tnmsc.csu.edu.cn/download/16-p0552-2024-0934-Supporting_Information.pdf.

References

[1] ZHANG Shu-jun, YU Fa-peng. Piezoelectric materials for high temperature sensors [J]. Journal of the American Ceramic Society, 2011, 94: 3153−3170.

[2] JIANG Xiao-ning, KIM K, ZHANG Shu-jun, JOHNSON J, SALAZAR G. High-temperature piezoelectric sensing [J]. Sensors, 2014, 14: 144−169.

[3] ZHANG Shu-jun, JIANG Xiao-ning, LAPSLEY M, MOSES P, SHROUT T R. Piezoelectric accelerometers for ultrahigh temperature application [J]. Applied Physics Letters, 2010, 96: 013506.

[4] YANG Wen-chao, QU Peng-fei, LIU Chen, CAO Kai-li, QIN Jia-run, SU Hai-jun, ZHANG Jun, REN Cui-dong, LIU Lin. Temperature dependence of compressive behavior and deformation microstructure of a Ni-based single crystal superalloy with low stacking fault energy [J]. Transactions of Nonferrous Metals Society of China, 2023, 33: 157−167.

[5] LUO Ya-jun, ZHANG Wei-dong, PENG Fei, LIU Sheng, LI Zhong-tao, WU Zheng-gang. Temperature dependence of mechanical properties of equiatomic NiCoCr medium-entropy alloy printed by selective laser melting [J]. Transactions of Nonferrous Metals Society of China, 2024, 34: 1547−1557.

[6] DAMJANOVIC D. Materials for high temperature piezoelectric transducers [J]. Current Opinion in Solid State and Materials Science, 1998, 3: 469−473.

[7] TURNER R C, FUIERER P A, NEWNHAM R E, SHROUT T R. Materials for high temperature acoustic and vibration sensors: A review [J]. Applied Acoustics, 1994, 41: 299−324.

[8] SHROUT T R, ZHANG Shu-jun. Lead-free piezoelectric ceramics: Alternatives for PZT?[J]. Journal of Electroceramics, 2007, 19: 113−126.

[9] PANDA P K. Review: Environmental friendly lead-free piezoelectric materials [J]. Journal of Materials Science, 2009, 44: 5049−5062.

[10] LIU Gang, YUAN Jing, NIE Rui, JIANG Lai-ming, TAN Zhi, ZHU Jian-guo, CHEN Qiang. Electrical properties and thermal stability of Ce-modified $Ca_{0.80}(Li_{0.5}Bi_{0.5})_{0.20}Bi_2Nb_2O_9$ ceramics [J]. Journal of Alloys and Compounds, 2017, 697: 380−387.

[11] NEWNHAM R E, WOLFE R W, DORRIAN J F. Structural basis of ferroelectricity in the bismuth titanate family [J]. Materials Research Bulletin, 1971, 6: 1029−1039.

[12] SUBBARAO E C. A family of ferroelectric bismuth compounds [J]. Journal of Physics and Chemistry of Solids, 1962, 23: 665−676.

[13] YAN Hai-xue, ZHANG Hong-tao, UBIC R, REECE M J, LIU Jing, SHEN Zhi-jian, ZHANG Zhen. A lead-free high-Curie-point ferroelectric ceramic, $CaBi_2Nb_2O_9$ [J]. Advanced Materials, 2005, 17: 1261−1265.

[14] CHEN Huan-bei, SHEN Bo, XU Jin-bao, KONG Ling-bing, ZHAI Ji-wei. Correlation between grain sizes and electrical properties of $CaBi_2Nb_2O_9$ piezoelectric ceramics [J]. Journal of the American Ceramic Society, 2012, 95: 3514−3518.

[15] FRIT B, MERCURIO J P. The crystal chemistry and dielectric properties of the Aurivillius family of complex bismuth oxides with perovskite-like layered structures [J]. Journal of Alloys and Compounds, 1992, 188: 27−35.

[16] PENG Zhi-hang, CHEN Qiang, LIU Dan, WANG Ya-dan, XIAO Din-quan, ZHU Jian-guo. Evolution of microstructure

and dielectric properties of (LiCe)-doped $Na_{0.5}Bi_{2.5}Nb_2O_9$ Aurivillius type ceramics [J]. Current Applied Physics, 2013, 13: 1183−1187.

[17] WANG Chun-ming, WANG Jin-feng, ZHANG Shu-jun, SHROUT T R. Piezoelectric and electromechanical properties of ultrahigh temperature $CaBi_2Nb_2O_9$ ceramics [J]. Physica Status Solidi (RRL) − Rapid Research Letters, 2009, 3: 49−51.

[18] WANG He-peng, JIANG Xiang-ping, CHEN Chao, HUANG Xiao-kun, NIE Xin, YANG Li, FAN Wen-ying, JIE Shao-tian, WANG Hui. Structure and electrical properties of Ce-modified $Ca_{1-x}Ce_xBi_2Nb_{1.75}(Cu_{0.25}W_{0.75})_{0.25}O_9$ high Curie point piezoelectric ceramics [J]. Ceramics International, 2022, 48: 1723−1730.

[19] WANG Dan, XU Yu-gen, SHI Yu-lin, WANG Hong-liang, WU Xiao-jun, WU Chao, ZHU Jian-guo, CHEN Qiang. The structure and electrical properties of $Ca_{0.6}(Li_{0.5}Bi_{0.5-x}Pr_x)_{0.4}$-$Bi_2Nb_2O_9$ high-temperature piezoelectric ceramics [J]. Journal of the American Ceramic Society, 2020, 103: 266−278.

[20] ZHU Cheng-hao, CHEN A-xaing, LIU Yang, ZHENG Peng, BAI Wang-feng, FAN Qiao-lan, ZHENG Liang, ZHANG Yang. Realizing enhanced electrical properties of $CaBi_2Nb_2O_9$-based high-temperature piezoceramics by constructing a pseudophase boundary [J]. ACS Applied Electronic Materials, 2022, 4: 3598−3605.

[21] WANG Fei, LI Xu, XU Qian, CHEN Ning, CHEN Hao, CHENG Yuan, ZHANG Fei-fei, TAN Zhi, XING Jie, CHEN Qiang, ZHU Jian-guo. Influence of acceptor-donor codoping on the structure, electrical properties, and hardness of $CaBi_2Nb_2O_9$-based ceramics [J]. Journal of Alloys and Compounds, 2022, 910: 164853.

[22] CHEN Zhen-ning, SHENG Lin-sheng, LI Xu-dong, ZHENG Peng, BAI Wang-feng, LI Li-li, WEN Fei, WU Wei, ZHENG Liang, CUI Jia-dong. Enhanced piezoelectric properties and electrical resistivity in W/Cr co-doped $CaBi_2Nb_2O_9$ high-temperature piezoelectric ceramics [J]. Ceramics International, 2019, 45: 6004−6011.

[23] CHEN A-xiang, CHEN Zhen-ning, LIU Yang, ZHENG Peng, BAI Wang-feng, LI Li-li, WEN Fei, ZHENG Liang, ZHANG Yang. Enhanced electrical properties in W/Cu co-doped $CaBi_2Nb_2O_9$ high-temperature piezoelectric ceramics [J]. International Journal of Applied Ceramic Technology, 2021, 18: 2111−2120.

[24] CHEN Zheng-ning, ZHANG Yu-hao, HUANG Pei-ming, LI Xu-dong, DU Juan, BAI Wang-feng, LI Li-li, WEN Fei, ZHENG Peng, WU Wei, ZHENG Liang, ZHANG Yang. Enhanced piezoelectric properties and thermal stability in Mo/Cr co-doped $CaBi_2Nb_2O_9$ high-temperature piezoelectric ceramics [J]. Journal of Physics and Chemistry of Solids, 2020, 136: 109195.

[25] SHEN Zong-yang, SUN Hua-jun, TANG Yan-xue, LI Yue-ming, ZHANG Shu-jun. Enhanced piezoelectric properties of Nb and Mn co-doped $CaBi_4Ti_4O_{15}$ high temperature piezoceramics [J]. Materials Research Bulletin, 2015, 63: 129−133.

[26] XING Xing-he, CAO Feng, PENG Zhi-hang, XIANG Yang. The effects of oxygen vacancies on the electrical properties of W, Ti doped $CaBi_2Nb_2O_9$ piezoceramics [J]. Current Applied Physics, 2018, 18: 1149−1157.

[27] LI Yi-guang, ZHOU Zhi-yong, LIANG Rui-hong, GAO Bo-tao, ZHOU Zheng-yang, DONG Xian-lin. A simple Bi^{3+} self-doping strategy constructing pseudo-tetragonal phase boundary to enhance electrical properties in $CaBi_2Nb_2O_9$ high-temperature piezoceramics [J]. Journal of the European Ceramic Society, 2022, 42: 2772−2780.

[28] PAN Cheng-bing, ZHAO Gao-zhao, LI Su-mei, WANG Jia-ming-zhu, YIN Li-hua, SONG Wen-hai, ZHU Xue-bin, YANG Jie, SUN Yu-ping. Effect of $BaO-2B_2O_3$ sintering aid on the structural and electrical properties of $CaBi_2Nb_2O_9$ high-temperature piezoelectric ceramic [J]. Journal of Applied Physics, 2021, 130: 244102.

[29] SUN Yuan-yuan, YANG Hua-bin, GUAN Shi-Bo, CAO Yin-han, JIANG Min-hong, LIU Xiao, CHEN Qiao-hong, LI Min-jin, XU Ji-wen. Strong piezoelectricity of Li_2CO_3-doped $BiFeO_3$–$BaTiO_3$–$Bi(Zn_{0.5}Ti_{0.5})O_3$ lead-free piezoelectric ceramics with high Curie temperature and high temperature stability [J]. Journal of Alloys and Compounds, 2020, 819: 153058.

[30] KIZAKI Y C, NOGUCHI Y J, MIYAYAMA M. Defect control for low leakage current in $K_{0.5}Na_{0.5}NbO_3$ single crystals [J]. Applied Physics Letters, 2006, 89: 142910.

[31] YANG Hua-bin, ZHOU Chang-rong, LIU Xin-yu, ZHOU Qin, CHEN Guo-hua, LI Wei-zhou, WANG Hua. Piezoelectric properties and temperature stabilities of Mn- and Cu-modified $BiFeO_3$-$BaTiO_3$ high temperature ceramics [J]. Journal of the European Ceramic Society, 2013, 33: 1177−1183.

[32] LEONTSEV S O, EITEL R E. Dielectric and piezoelectric properties in Mn-modified $(1-x)BiFeO_3$–$xBaTiO_3$ ceramics [J]. Journal of the American Ceramic Society, 2009, 92: 2957−2961.

[33] LUO Feng, LI Zhi-Min, CHEN Ji-yuan, YAN Yang-xi, ZHANG Dong-yan, ZHANG Mao-lin, HAO Yue. High piezoelectric properties in $0.7BiFeO_3-0.3BaTiO_3$ ceramics with MnO and MnO_2 addition [J]. Journal of the European Ceramic Society, 2022, 42: 954−964.

[34] WANG Tao, JIANG Min-hong, LI Lin, CHENG Shuai, LU Huan, REN Peng-han, ZHAO Yan-guang, RAO Guang-hui. Effects of MnO_2-doping on growth, structure and electrical properties of lead-free piezoelectric $K_{0.5}Na_{0.5}NbO_3$–$BiAlO_3$ single crystals [J]. Journal of Alloys and Compounds, 2023, 935: 168126.

[35] KIM D J, LEE M H, SONG T K. Comparison of multi-valent manganese oxides (Mn^{4+}, Mn^{3+}, and Mn^{2+}) doping in $BiFeO_3$–$BaTiO_3$ piezoelectric ceramics [J]. Journal of the European Ceramic Society, 2019, 39: 4697−4704.

[36] JIANG Xing-an, JIANG Xiang-ping, CHEN Chao, TU Na, CHEN Yun-jing, ZHANG Ban-chao. Photoluminescence and electrical properties of Eu^{3+}-doped $Na_{0.5}Bi_{4.5}Ti_4O_{15}$-based ferroelectrics under blue light excitation [J]. Frontiers of Materials Science, 2016, 10: 31−37.

[37] FAN Gang, JIANG Xiang-ping, CHEN Chao, CHEN Yun-jing, DU Ke-yi, TU Na, JIANG Xing-an, XIA Xiang, WANG Peng-bin. Photoluminescence and electrical properties of Eu^{3+} doped $CaBi_8Ti_7O_{27}$ intergrowth ceramics [J]. Journal of Materials Science: Materials in Electronics, 2018, 29: 6484−6490.

[38] LIU Gang, REN Sheng-qiang, WU Chao, WANG Dan, LI Feng-lian, WU Jia-gang, CHEN Qiang. Enhanced thermal stability of (NaCe)-multidoped $CaBi_2Nb_2O_9$ by A-site vacancies-induced pseudo-tetragonal distortion [J]. Journal of the American Ceramic Society, 2018, 101: 4615−4626.

[39] JEON M K, KIM Y I, NAHM S H, WOO S I. Combined structural refinement of $Bi_{3.5}La_{0.5}Ti_3O_{12}$ using neutron and X-ray powder diffraction data [J]. The Journal of Physical Chemistry B, 2005, 109: 968−972.

[40] DIAO Chun-li, XU Jian-bin, ZHENG Hai-wu, FANG Liang, GU Yu-zong, ZHANG Wei-feng. Dielectric and piezoelectric properties of cerium modified $BaBi_4Ti_4O_{15}$ ceramics [J]. Ceramics International, 2013, 39: 6991−6995.
[41] SHIMANSKIJ A F, DROFENIK M, KOLAR D. Subsolidus grain growth in donor doped barium titanate [J]. Journal of Materials Science, 1994, 29: 6301−6305.
[42] LIU Yi-xuan, LI Zhao, THONG Hao-cheng, LU Jing-tong, LI Jing-feng, GONG Wen, WANG Ke. Grain size effect on piezoelectric performance in perovskite-based piezoceramics [J]. Acta Physica Sinica, 2020, 69: 217704. (in Chinese)
[43] ZHUK N A, LUTOEV V P, MAKEEV B A, NEKIPELOV S V, KOROLEVA A V, FEDOROVA A V, YERMOLINA M V, BEZNOSIKOV D S, KARLOVA L O. Magnetic susceptibility, EPR, NEXAFS and XPS spectra of Fe-doped $CaBi_2Nb_2O_9$ [J]. Journal of Materials Research and Technology, 2020, 9: 4173−4182.
[44] ZOU Wei, WANG Jian-lin, CHEN Ze-zhi, SHI Nai, LI Zhi-ang, CUI Zhang-zhang, LI Xiao-ning, YIN Xiao-feng, YAN Wen-sheng, HUANG Hao-liang, PENG Ran-ran, FU Zheng-ping, LU Ya-lin. Anisotropic electrical and magnetic properties in grain-oriented $Bi_4Ti_3O_{12}$−$La_{0.5}Sr_{0.5}MnO_3$ [J]. Journal of Materials Chemistry C, 2018, 6: 11272−11279.
[45] WANG Fei, LI Xu, XU Qian, CHEN Hao, XI Jing-wen, ZHANG Fei-fei, TAN Zhi, CHENG Yuan, WANG Shi-fa, XING Jie, CHEN Qiang, ZHU Jian-guo. Simultaneous enhancement of electrical and mechanical properties in $CaBi_2Nb_2O_9$-based ceramics [J]. Journal of the European Ceramic Society, 2022, 42: 4196−4211.
[46] FU Jian, XIE Ai-wen, LI Tian-yu, ZOU Ru-zhong. Ultrahigh piezoelectricity in (Ba,Ca)(Ti,Sn)O_3 lead-free compounds with enormous domain wall contribution [J]. Acta Materialia, 2022, 230: 10233−10241.
[47] SUÁREZ D Y, REANEY I M, LEE W E. Relation between tolerance factor and *Tc* in Aurivillius compounds [J]. Journal of Materials Research, 2001, 16: 3139−3149.
[48] YAN Hai-xue, ZHANG Hong-tao, REECE M J, DONG Xian-lin. Thermal depoling of high Curie point Aurivillius phase ferroelectric ceramics [J]. Applied Physics Letters, 2005, 87: 082911.
[49] ZHANG Man, CHEN Zhe, YUE Ya-jun, CHEN Tao, YAN Zhong-na, JIANG Qing-hui, YANG Bin, ERIKSSON M, TANG Jian-hua, ZHANG Dou, SHEN Zhi-jian, ABRAHAMS I, YAN Hai-xue. Terahertz reading of ferroelectric domain wall dielectric switching [J]. ACS Applied Materials & Interfaces, 2021, 13: 12622−12628.
[50] YU Hong-cai, HOU Qing-quan, CHEN Gong-tian, MA Chao, JIANG Xing-an, HONG Jia-wang, ZHOU Zhi-yong, LIANG Rui-hong, DONG Xian-lin, XIAO Han-ning, YANG Bin. Ternary doping of Na^+, $Bi^{3+}$and La^{3+} to improve piezoelectric constant and electrical resistivity simultaneously in calcium bismuth niobate ceramics [J]. Ceramics International, 2023, 49: 10738−10747.
[51] PAN Cheng-bing, ZHAO Gao-chao, LI Su-mei, SHU Ming-fang, WU Jie, WANG Jia-ming-zhu, YIN Li-hua, SONG Wen-hai, ZHU Xue-bin, YANG Jie, SUN Yu-ping. Enhanced electrical properties in Ce/Mo co-substituted $CaBi_2Nb_2O_9$ high-temperature piezoelectric ceramic [J]. Journal of Materials Science: Materials in Electronics, 2021, 32: 19938−19946.
[52] CHEN Huan-bei, GUO Xiang-xin, CUI Zhong-hui, ZHAI Ji-wei. Donor and acceptor doping effects on the electrical conductivity of $CaBi_2Nb_2O_9$ ceramics [J]. Physica Status Solidi (a), 2013, 210: 1121−1127.
[53] ZHANG Hong-tao, YAN Hai-xue, REECE M J. The effect of Nd substitution on the electrical properties of Bi_3NbTiO_9 Aurivillius phase ceramics [J]. Journal of Applied Physics, 2009, 106: 044106.
[54] SHULMAN H S, TESTORF M, DAMJANOVIC D, SETTER N. Microstructure, electrical conductivity, and piezoelectric properties of bismuth titanate [J]. Journal of the American Ceramic Society, 1996, 79: 3124−3128.
[55] PENG Zhi-hang, CHEN Li, XIANG Yang, CAO Feng. Microstructure and electrical properties of lanthanides-doped $CaBi_2Nb_2O_9$ ceramics [J]. Materials Research Bulletin, 2022, 148: 111670.

MnO_2 掺杂提高 $CaBi_2Nb_2O_9$ 压电陶瓷的压电性能和居里温度

王梦思[1]，张 妍[1]，罗小刚[1]，汤 林[1]，向 珊[1]，郭 茹[2]，周学凡[1]，周科朝[1]，张 斗[1]

1. 中南大学 粉末冶金国家重点实验室，长沙 410083；
2. 香港中文大学 机械与自动化系，香港 999077

摘 要：通过固相烧结法制备 MnO_2 掺杂的 $Ca_{0.97}Bi_{2.03}Nb_2O_9$ 陶瓷，其压电性能得到了显著提升。研究 MnO_2 掺杂对 $Ca_{0.97}Bi_{2.03}Nb_2O_9$ 陶瓷显微组织和电学性能的影响。X 射线衍射(XRD)分析及 Rietveld 精修结果表明，MnO_2 的掺杂降低了正交畸变程度，从而有助于提高压电性能。此外，MnO_2 的引入降低了烧结温度，从而抑制了陶瓷中氧空位的形成。性能最优的样品为 $Ca_{0.97}Bi_{2.03}Nb_2O_9$−0.3%$MnO_2$(质量分数)，其压电系数($d_{33}$) 达到 13.6 pC/N，在 500 ℃时的直流电阻率为 3×10^6 Ω·cm，居里温度为 965 ℃。另外，所有掺杂样品在室温至 900 ℃的宽温度范围内均表现出优异的热稳定性

关键词：铌酸铋钙陶瓷；MnO_2 掺杂；晶体结构；氧空位

(Edited by Xiang-qun LI)